catalysts

MDPI

Article

Tuning Lanthanum Promotion in Ni/CeO_2 Catalysts for Hydrogen-Rich Syngas Production via Partial Oxidation of Methane

Wedad A. Al-onazi [1], Abdulaziz A. M. Abahussain [2,*], Tahani Saad Algarni [1], Mohammed F. Alotaibi [3], Mohammed O. Bayazed [2], Rehab M. Ali [2], Alaaddin M. M. Saeed [4], Khalid M. Alshamrani [3], Rawesh Kumar [5] and Ahmed S. Al-Fatesh [2,*]

1 Department of Chemistry, College of Science, King Saud University, P.O. Box 2455, Riyadh 11451, Saudi Arabia
2 Department of Chemical Engineering, College of Engineering, King Saud University (KSU), P.O. Box 800, Riyadh 11421, Saudi Arabia; rehabmohamedali1988@gmail.com (R.M.A.)
3 Institute of Refining and Petrochemicals Technologies, King Abdulaziz City for Science and Technology (KACST), P.O. Box 6086, Riyadh 11442, Saudi Arabia; mfalotaibi@kacst.gov.sa (M.F.A.)
4 United Chemical Reaction Engineering Research Institute, State Key Laboratory of Chemical Engineering, East China University of Science and Technology, Shanghai 200237, China
5 Department of Chemistry, Patna University, Patna 800005, Bihar, India
* Correspondence: a.abahussain@ksu.edu.sa (A.A.M.A.); aalfatesh@ksu.edu.sa (A.S.A.-F.)

Abstract

Partial oxidation of methane (POM) provides an efficient route to convert methane into hydrogen-rich syngas, with lower energy demands than conventional steam reforming. This work evaluates lanthanum promotion effects on the physicochemical properties and catalytic behaviour of Ni/CeO_2 catalysts. A series of 5Ni + xLa/CeO_2 catalysts with 0–2 wt.% La was synthesised by wetness impregnation and characterized using N_2 adsorption–desorption, Raman spectroscopy, and cyclic H_2-TPR–O_2-TPO–H_2-TPR analysis. The results proved that promoter La has a strong effect on the structure and surface chemistry of the Ni/CeO_2 catalysts, as it modifies the CeO_2 framework, encourages the formation of surface carbonate species, and changes Ni interaction with the support. These structural shifts are closely tied to the enhancement of the catalyst's performance and stability during POM. Among the catalysts, 5Ni + 1.5La/CeO_2 struck the best balance between textural properties and catalytic performance. At 600 °C and a GHSV of 14,400 mL h^{-1} $g_{cat}{}^{-1}$, the CH_4 conversion reached about 57–59% and H_2 yield reached 53–55% over 300 min on stream. It also led to more than 70% CH_4 conversion and more than 65% H_2 yield for 22 h at 600 °C and 7200 mL h^{-1} g_cat^{-1}, showing sustainable hydrogen-rich syngas production during continuous operation. However, increasing the La loading to 2 wt.% strengthened the La–CeO_2 interaction to the point of limiting the accessibility and dispersion of active sites, which lowered catalytic activity. Hence, these findings reveal that 1.5 wt.% La is the optimum loading, which balances support structure, metal–support interaction, surface chemistry, and active-site accessibility, and offers a practical strategy for producing more effective and stable Ni/CeO_2 catalysts for hydrogen-rich syngas production via POM.

Keywords: partial oxidation of methane; Ni-catalyst; lanthanum promoter; CeO_2 support; cyclic H_2-TPR–O_2-TPO–H_2-TPR

Check for updates

Academic Editor: Hongxing Dai

Received: 1 October 2026
Revised: 25 October 2026
Accepted: 26 October 2026
Published: 28 October 2026

Copyright: © 2026 by the authors. Licensee MDPI, Basel, Switzerland. This article is an open access article distributed under the terms and conditions of the Creative Commons Attribution (CC BY) license.

1. Introduction

Methane is both a major climate liability and an underutilized carbon resource [1]. As the primary component of natural gas, CH_4 is available on a large scale, yet its atmospheric

release has disproportionate climate consequences because fossil methane has a 20-year global warming potential of 82.5 and a 100-year global warming potential of 29.8 relative to CO_2 [2]. Methane has also contributed approximately 30% of the global temperature increase since the Industrial Revolution [3]. Thus, the utilization of captured methane can serve a dual function: mitigating point-source methane emissions and providing a direct catalytic route to transform an inexpensive C_1 carbon source into valuable products.

Catalytic valorisation of CH_4 therefore addresses both dimensions simultaneously by transforming natural gas into synthesis gas, a mixture of H_2 and CO that serves as a platform for Fischer–Tropsch fuels, methanol, hydrogen production, and downstream ammonia synthesis [4].

Among methane-to-syngas technologies, steam reforming of methane (SRM), dry reforming of methane (DRM), and partial oxidation of methane (POM) differ substantially in thermodynamic demand and product composition. SRM and DRM are strongly endothermic, whereas POM is mildly exothermic ($\Delta H° = -36$ kJ mol^{-1}) and produces syngas with an H_2/CO ratio close to 2. Compared with SRM, POM offers an estimated 10–15% reduction in energy requirements [5,6]. These features give POM practical advantages over conventional reforming processes, including lower energy demand.

Among the catalysts investigated for POM, noble-metal and Ni-based systems have attracted the most attention; however, Ni-based catalysts are particularly favoured owing to the earth-abundant nature of nickel, its low cost, and its intrinsic activity toward C–H bond activation. However, restricting Ni in metallic Ni in the presence of oxidizing gas feed like molecular oxygen is quite difficult, and partial oxidation of metallic Ni into NiO can be expected. The mixture of NiO and Ni catalyses methane into syngas through an indirect route, which can be summarized as the combustion of methane by molecular oxygen over NiO followed by reforming of methane by combustion products (CO_2 and H_2O) over metallic Ni into syngas (Figure 1). The reforming of methane by water theoretically produces syngas with an H_2/CO ratio of 3. The presence of water offers the significance of the water gas shift reaction, where water is reduced into hydrogen by carbon monoxide (one of the constituents of syngas), which results in further enrichment of hydrogen proportion in the syngas. These indirect reaction pathways may therefore increase the H_2/CO ratio above the stoichiometric ratio of 2 expected from direct POM.

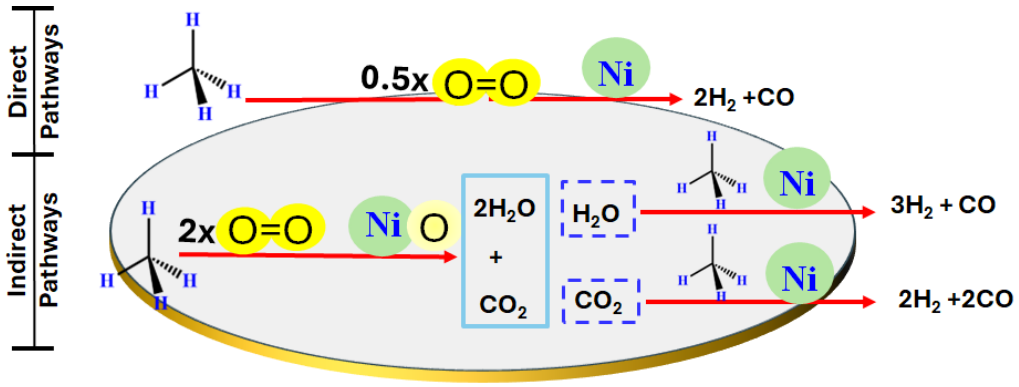


Figure 1. Reaction scheme of direct and indirect pathways of POM.

It should be noted that excessive oxidation of Ni in the presence of molecular oxygen can promote complete methane combustion frequently. Atomically dispersed MoNi alloy catalysts have shown that tuning oxygen adsorption on Ni suppresses over-oxidation and improves syngas selectivity [7]. Another limitation of the Ni-based catalyst system is metal sintering at high reaction temperatures. Controlling over-oxidation and restricting metal sintering require a careful selection of both the support material and promoter.

CeO_2 is not a passive support in methane partial oxidation; the Ce^{4+}/Ce^{3+} redox couple in the ceria lattice provides mobile lattice oxygen, which may promote gasification of coke and enables facile oxygen vacancy formation, which can assist C–H bond activation [8,9]. Ni incorporation into CeO_2 generates interfacial and surface defects, including Ni–O–Ce-type structures, which facilitate methane activation [10] and may enhance POM activity [11]. More broadly, Ni–oxygen vacancy interfaces have been reported to improve the reducibility, strengthen metal–support interaction, and suppress carbon accumulation in methane reforming chemistry, which reinforces the role of CeO_2-derived oxygen vacancies as functional sites rather than simple structural defects [12,13].

Direct evidence for La-containing POM catalysts is provided by Ni/La_2O_3-modified biomass fly ash, where La_2O_3 addition improved CH_4 conversion from 55% to 85% and increased the H_2/CO ratio from 1.4 to 2, with stable operation over 30 h at 850 °C [14]. In related methane reforming systems, La-modified Ni catalysts show a clear loading-dependent behaviour where moderate La-loading improves carbon resistance and Ni dispersion, while excessive La-loading can reduce active-site accessibility, increase Ni particle size, and weaken the balance between surface exposure and dispersion [15]. This optimum-promoter concept is further supported by Ce-modified La-containing perovskite catalysts, where moderate Ce-loading promotes Ni exsolution and oxygen-vacancy formation, but excess CeO_{2-x} can cover metallic Ni sites and suppress activity [16]. As a basic oxide, La_2O_3 increases the density of basic sites that can adsorb CO_2 and promote carbon removal through lanthanum oxycarbonate chemistry, in which $La_2O_2CO_3$ participates in the gasification of surface carbon and helps regenerate La_2O_3-type basic sites. These studies establish that La loading must be optimized to balance basicity, oxygen-vacancy formation, Ni^0 exposure, and coke resistance, and that the optimal loading is system-specific.

Despite the demonstrated roles of La_2O_3 in modifying basicity, oxygen vacancy density, and carbon resistance in Ni-based methane conversion catalysts, a systematic investigation of the effect of La loading on 5 wt.% Ni/CeO_2 catalysts for POM at 600 °C has not been reported. Therefore, the relationship between La content, Ni^0 accessibility, CeO_2 redox behaviour, oxygen-vacancy formation, carbon resistance, and time-on-stream stability over $5Ni/CeO_2$ remains insufficiently understood under moderate-temperature POM conditions.

Herein, a series of La-promoted Ni/CeO_2 catalysts, denoted as $5Ni + xLa/CeO_2$ with x = 0, 0.5, 1, 1.5, and 2 wt.% La, was investigated for POM. The catalysts are characterized using N_2 adsorption–desorption analysis, X-ray diffraction, Raman spectroscopy, and cyclic H_2-temperature programmed reduction-O_2-oxidation-reduction experiment. The influence of La loading on the physicochemical properties, redox behaviour, and POM performance of Ni/CeO_2 was investigated. The fine tuning between characterization results and catalytic activity is established, which recommends the use of optimum loading of lanthanum over Ni/CeO_2 for consistent production of hydrogen rich syngas over a long period of streaming through the POM reaction.

2. Results

2.1. Textural Properties of the Catalysts

The N_2 adsorption–desorption isotherms and pore-size distributions of the reduced catalysts are presented in Figure 2, while the corresponding textural properties are summarized in Table 1. All catalysts exhibit a typical type IV adsorption isotherm with an H1 hysteresis loop, characteristic of a mesoporous framework of uniform cylindrical pores. The sharp increase in adsorbed volume at high relative pressure ($p/p^\circ > 0.8$) further confirms the presence of mesoporosity and a well-defined pore network in all samples. The pore-size distribution of all La-promoted catalysts reveals a narrow and unimodal distribution with average pore diameters in the 16–23 nm range, which further supports the

mesoporous nature inferred from the isotherms. The reduced-5Ni/CeO_2 catalyst exhibits 35 m^2/g BET surface area, 0.21 cm^3/g pore volume, and ~20 nm average pore diameter. Upon incorporation of 0.5 wt.% La, both the surface area and pore volumes of the catalyst decreased markedly, which may have resulted from the deposition of lanthanum species in the pores of the catalyst, which partially block the mesoporous channels. Among the La-promoted catalysts, the minimum reduction in surface area and pore volume is detected for reduced-5Ni + 1.5La/CeO_2 catalyst. It indicates better dispersion of Ni over the support in the presence of 1.5 wt.% La. 5Ni + 1.5La/CeO_2 and 5Ni + 2La/CeO_2 share the largest average pore width (26.7 nm), while 5Ni + 1.5La/CeO_2 distinctly possesses the highest pore volume (0.19 cm^3/g), which may also facilitate easier transport of gases and removal of carbon deposits across the pore channels of the catalyst, thereby enhancing catalytic performance and stability.

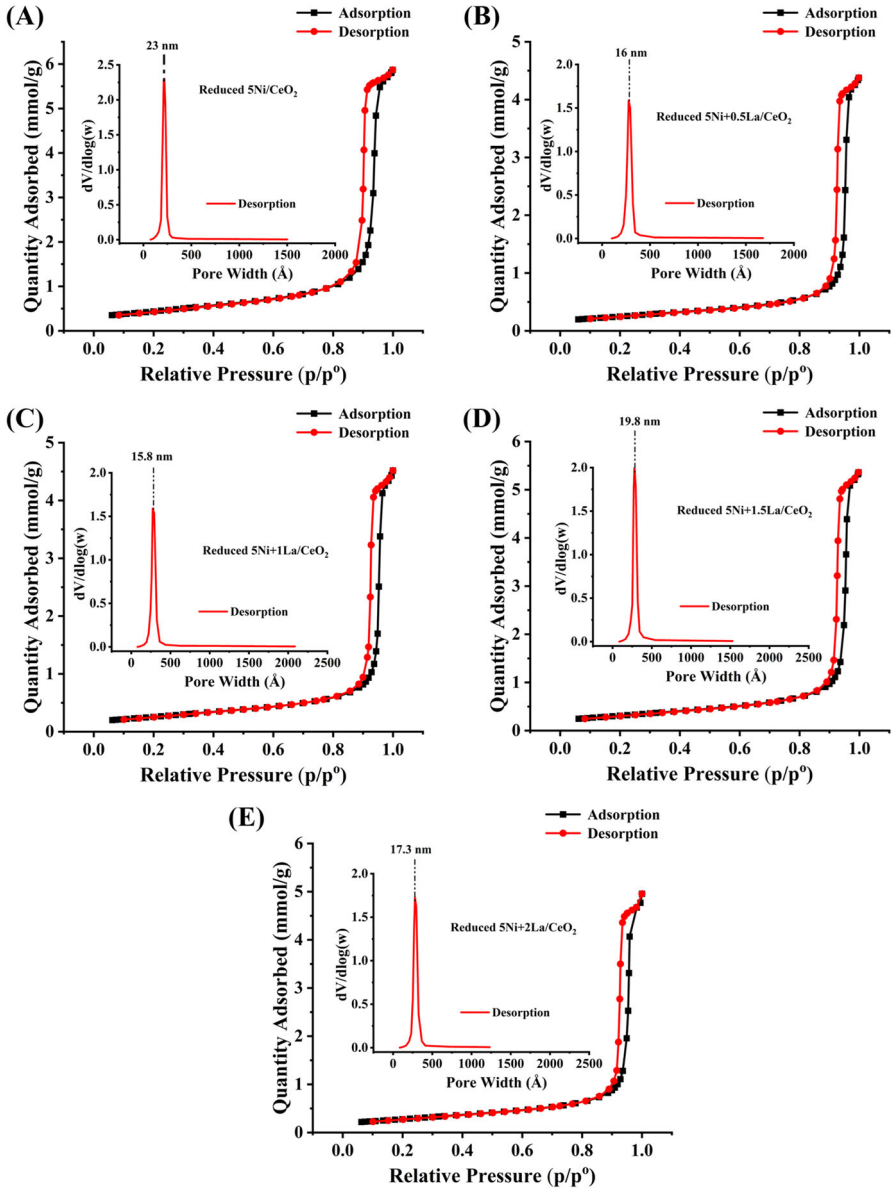


Figure 2. N_2-adsorption-desorption profiles of (**A**) 5Ni/CeO_2 (**B**) 5Ni + 0.5La/CeO_2 (**C**) 5Ni + 1La/CeO_2 (**D**) 5Ni + 1.5La/CeO_2 (**E**) 5Ni + 2La/CeO_2.

Table 1. Textural properties of the reduced unpromoted and La-promoted Ni/CeO_2 catalysts.

Catalyst Name	Surface Area (m^2/g)	Pore Volume (cm^3/g)	Average Pore Diameter (nm)
Reduced-5Ni/CeO_2	35.0	0.21	20.2
Reduced-5Ni + 0.5La/CeO_2	20.0	0.16	26.6
Reduced-5Ni + 1La/CeO_2	21.0	0.16	26.6
Reduced-5Ni + 1.5La/CeO_2	25.0	0.19	26.7
Reduced-5Ni + 2La/CeO_2	22.6	0.17	26.7

The equal pore diameter of 5Ni + 1.5La/CeO_2 and 5Ni + 2La/CeO_2 is distinguished by their differing pore volumes.

2.2. The X-Ray Diffraction (XRD) Analysis

The X-ray diffraction (XRD) patterns of the reduced catalysts are presented in Figure 3A,B, and their full range figure is supplied in the Supplementary Data (Figure S2). The diffraction patterns confirm the presence of a cubic fluorite ceria phase in all catalysts. The reflections corresponding to the (111), (200), (220), and (311) crystalline planes of cubic ceria are detected at approximately 2θ of 28.6, 33.3, 47.8, and 56.9, whereas the weaker reflections of the (222), (400), (331), (420), (422), and (511) planes are observed at 59.6, 69.6, 76.8, 79, 88.5, and 95.5, respectively (JCPDS reference number 00-001-0800). No diffraction peaks corresponding to crystalline La-related or metallic Ni-related phases are detected, which suggests that these species are either highly dispersed or present predominantly in an amorphous form. It is interesting to note that the CeO_2 crystalline plane intensity increases with La addition to reach a maximum at 1 wt.% lanthanum loading, which indicates an increase in the CeO_2 crystallinity. A further increase in La loading drops the peak intensities to a minimum for the 5Ni + 2La/CeO_2 catalyst.

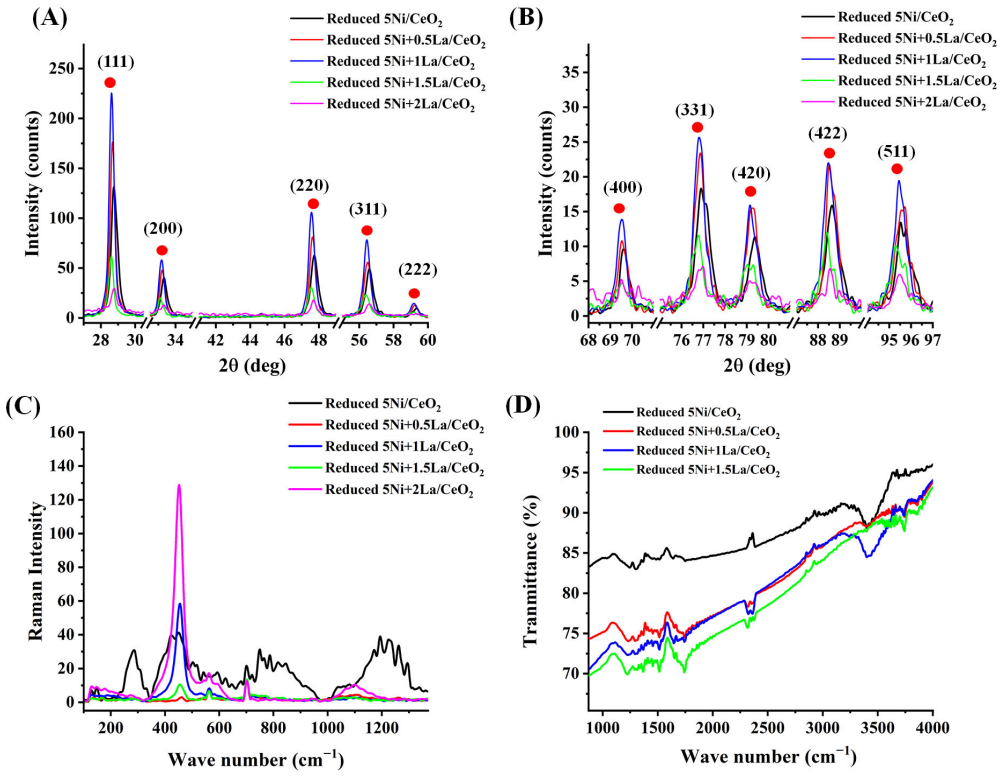


Figure 3. XRD patterns of the reduced $5Ni/CeO_2$ and 5Ni + xLa/CeO_2 (x = 0.5, 1, 1.5, and 2 wt.%) catalysts in the 2θ ranges of (**A**) 27–60°; (**B**) 68–97°. The red circles indicate reflections associated with the cubic fluorite CeO_2 phase; (**C**) Raman and (**D**) FT-IR of the reduced $5Ni/CeO_2$ and 5Ni + xLa/CeO_2 (x = 0.5, 1, 1.5, and 2 wt.%) catalysts.

2.3. Raman Spectroscopic Analysis

The Raman spectra of the reduced catalysts are presented in Figure 3C. The reduced 5Ni/CeO_2 sample shows vibration peaks at about 280, 465, 800, and 1098 cm^{-1}. The peak at about 280 cm^{-1} appears due to doubly degenerate transverse optical (TO) mode of ceria lattice [17]. The sharp peak at about 465 cm^{-1} is attributed to the F_2g Raman-active mode of fluorite CeO_2 lattice, which generates from the symmetric vibration of oxygen atoms surrounding the Ce cations [18,19]. The broad peak at about ~800 cm^{-1} of peroxide stretching O–O (O_2^{2-}) formed on ceria surfaces is also observed in the reduced 5Ni/CeO_2 catalyst [20]. The broad feature at 1098 cm^{-1} is attributed to the higher-order longitudinal optical (LO) vibration mode of CeO_2. Upon addition of 0.5 wt.% La, the vibration peak intensity of catalysts is largely suppressed, indicating significant modification of the CeO_2 support structure by La. Interestingly, the intensity of the F_2g vibration peak at about 465 cm^{-1} varies considerably with La loading. Therefore, the Raman results provide evidence of the strong interaction between La and the CeO_2 support.

2.4. Infrared Spectroscopic Analysis

The infrared spectra of reduced catalysts are presented in Figure 3D. Interestingly, upon addition of La, the IR band at about 1518 and 1739 cm^{-1} are intensified, which is attributed to unidentate carbonate coordinated to La^{+3} and bidentate chemisorbed CO_2 respectively [21]. Clearly in the presence of lanthana, the catalyst surface is enriched with CO_2-intermediate surface species, which may also trigger the indirect pathways of POM, namely combustion of methane followed by dry reforming of methane.

2.5. Redox Property of the Catalysts

In the POM reaction, the catalyst is reduced under hydrogen prior to the reaction, and then the POM's gas feed (made up of CH_4 and O_2) is allowed to pass through the catalyst surface at a given temperature. As the POM reaction proceeds, hydrogen rich syngas is evolved out. It should be noted that molecular oxygen (in the reactant gas feed) also oxidizes the metallic Ni, and molecular hydrogen (in evolving gas in POM) also helps retain the metallic Ni. Therefore, the reduction profile of the catalyst in the presence of molecular oxygen and hydrogen needs to be explained. For this purpose, the catalyst is reduced under hydrogen (through H_2-TPR), then oxidized by oxygen (through O_2-TPO), and again reduced by hydrogen (through H_2-TPR). This experiment is termed cyclic H_2TPR-O_2TPO-H_2TPR, as presented in Figure 4. The first H_2-TPR (in the cyclic experiment) of every catalyst is composed of a reduction peak at about ~230 °C (for reduction of free NiO), ~300 °C (for reduction of interacted-NiO), and 800 °C (for reduction of bulk ceria) [22]. After exposure of oxygen (through O_2-TPO) and subsequent reduction under hydrogen (last H_2-TPR), the reduction profile of the catalysts is greatly modified. The reduction peak of free NiO has disappeared completely. Each catalyst shows two intense reduction peaks centered at about 350 and 800 °C. In the last H_2-TPR, the reduction peak in the intermediate temperature region is shifted to a higher temperature, indicating enhanced metal–support interaction. This indicates that the sequential reduction-oxidation treatment causes enhanced metal–support interaction over all catalysts in the POM reaction. It is noted that the reduction profile of the catalyst is not varied much upon addition of different amounts of lanthanum promoter. Table S1 displays the H_2-consumption of the catalysts.

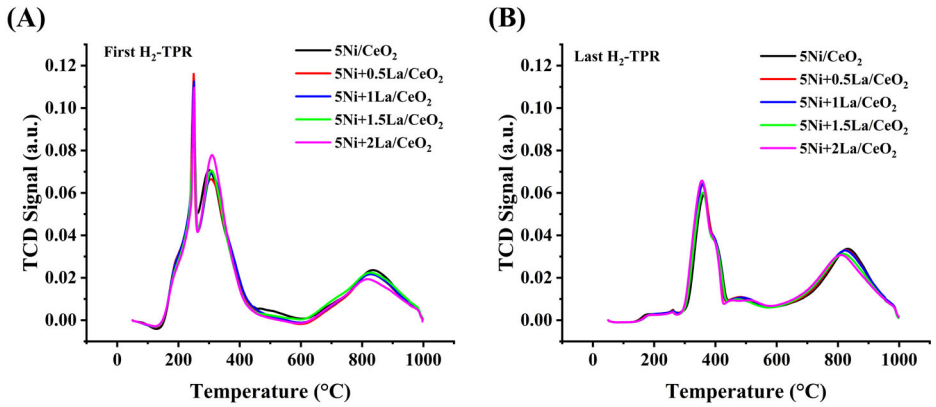


Figure 4. (**A**) First H_2 TPR of 5Ni + xLa/CeO_2 (x = 0.0, 0.5, 1, 1.5, 2) catalysts and (**B**) last H_2 TPR of 5Ni + xLa/CeO_2 (x = 0.0, 0.5, 1, 1.5, 2) catalysts.

2.6. Catalytic Activity

The catalytic activity and product yields of the 5Ni/CeO_2 and La-promoted catalysts during POM at 600 °C are presented in Figure 5. As discussed in Section 2.5, over the ceria supported Ni catalyst, the interaction of Ni with the support grows during the reduction–oxidation–reduction cycle in POM reaction. The H_2/CO ratio over each catalyst was found to be greater than 2.6, indicating the presence of parallel reactions, which may enrich the H_2 proportion in syngas. These parallel reactions may include indirect pathways of POM (which are catalyzed by a set of NiO and Ni) and water gas shift reaction. Lanthanum loading ≥1.5 wt.% shows an initial higher H_2/CO ratio than other catalysts. The consistent evolution of syngas was observed over a moderate lanthanum loaded catalyst (<1.5 wt.% La) and unpromoted catalysts after 90 min of reaction. The degree of graphitization of (I_D/I_G) of spent catalysts is found to be >1, indicating the deposit of more disordered carbon than ordered carbon during the POM reaction (Figure S3).

The unpromoted catalyst achieved about 49–51% CH_4 conversion and yielded 45–46% H_2 during 300 min in POM reaction at 14,400 mL h^{-1} $g_{cat}{}^{-1}$ gas hourly space velocity (GHSV) and 600 °C reaction temperature. IR results show the unique presence of "unidentate carbonate coordination of La^{+3}" and "bidentate chemisorbed CO_2" over the La-promoted catalyst, which potentially engages the CO_2 (if it is formed during the combustion of methane) in the oxidation of CH_4 through indirect pathways. The potential utilization of both direct and indirect pathways results in enhanced catalytic activity over La-promoted catalyst compared to the un-promoted catalyst. These results clearly show the promotional role of lanthanum over ceria-supported Ni-catalyst towards POM reaction. Surface parameters like surface area and pore dimension are comparable in reduced 5Ni + 0.5La/CeO_2 and reduced 5Ni + 1La/CeO_2 catalysts. After 60 min of reaction, both catalysts also show comparable activity (54–56% CH_4 conversion and 50–51% H_2 yield) for up to 300 min of reaction. The higher loading of lanthana (≥1.5 wt.%) makes the catalyst less crystalline and more amorphous. A total of 1.5 wt.% lanthanum loading was found to be optimal, as this catalyst exhibited the largest surface parameter as well as the highest catalytic activity compared to the rest of the promoted catalysts. The 5Ni + 1.5La/CeO_2 catalyst converted about 57–59% CH_4 and yielded 53–55% H_2 during 300 min time on stream at 14,400 mL h^{-1} $g_{cat}{}^{-1}$ GHSV and 600 °C. Upon decreasing the GHSV from 14,400 to 7200 mL h^{-1} $g_{cat}{}^{-1}$ over 5Ni + 1.5La/CeO_2, the contact time between the catalyst and the reaction feed is increased, which results in a consistent rise of catalytic activity. At 7200 mL h^{-1} $g_{cat}{}^{-1}$ GHSV, the 5Ni + 1.5La/CeO_2 catalyst attains > 70% CH_4 conversion and >65% H_2 yield at 600 °C reaction temperature (Figure 5E). This performance remains consistent up to 22 h of reaction time at 7200 mL h^{-1} $g_{cat}{}^{-1}$ GHSV and 600 °C reaction

temperature (Figure 5F). Over spent 5Ni + 1.5La/CeO_2, the I_D/I_G ratio of coke is found to be 1.09 after 300 min and 1.00 after 22 h of POM reaction. That means the degree of graphitization of coke does not change markedly after a long period on stream (compared to the tested time on stream of 300 min) (Figures S3 and S4).

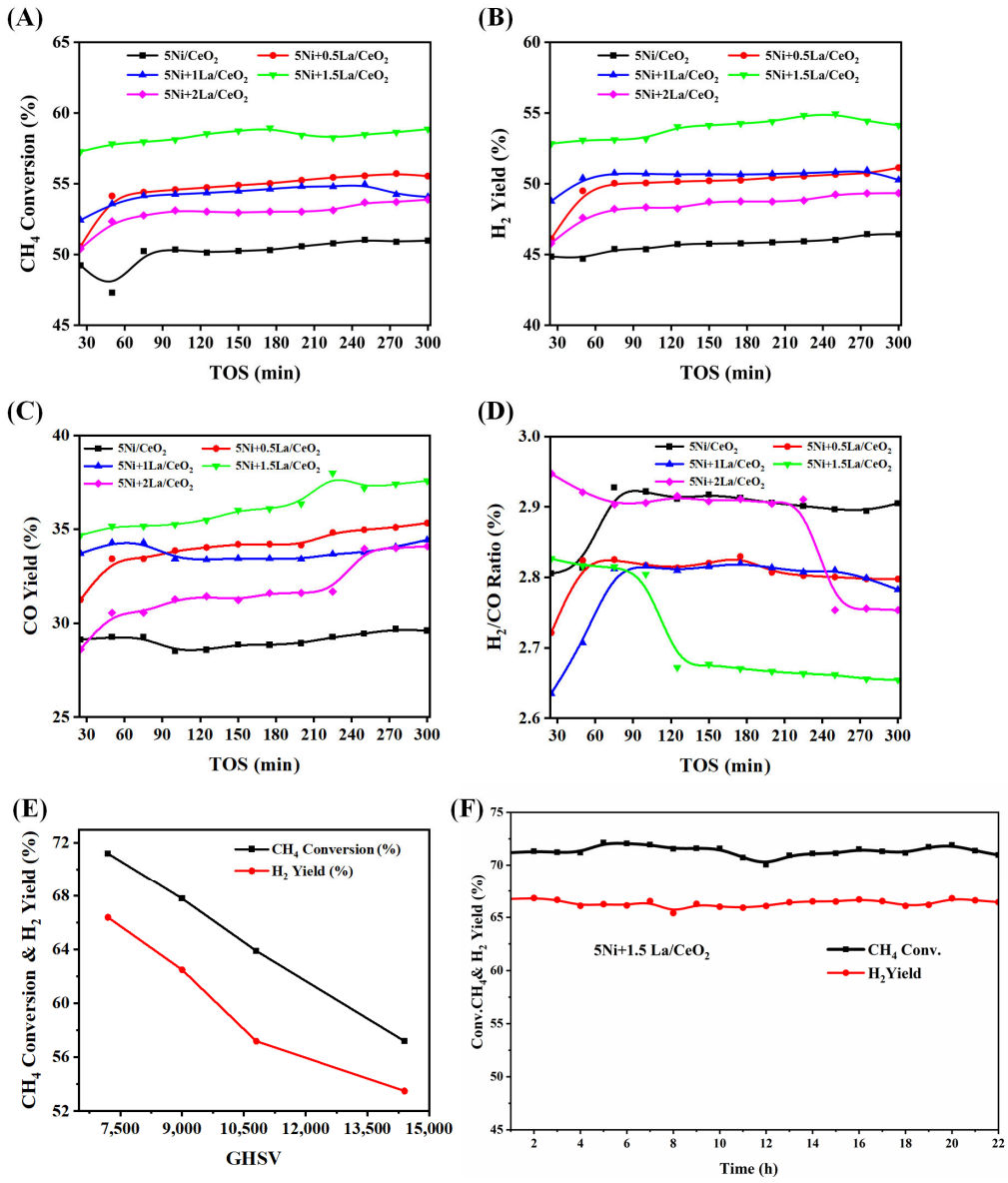


Figure 5. Catalytic activity results in 5Ni/CeO_2 and 5Ni + xLa/CeO_2 (x = 0.5, 1, 1.5, 2) catalysts at 14,400 mL h^{-1} g_{cat}^{-1} GHSV for: (**A**) CH_4 conversion v/s TOS, (**B**) H_2 yield v/s TOS, (**C**) CO yield v/s TOS, (**D**) H_2/CO ratio v/s TOS, (**E**) CH_4 conversion and H_2 yield v/s GHSV, and (**F**) CH_4 conversion and H_2 yield v/s TOS (long period under study) at 7200 mL h^{-1} g_{cat}^{-1} GHSV.

After optimal loading of lanthanum (5Ni + 2La/CeO_2), the crystallinity of the catalyst is decreased to a minimum, and the Raman vibration of the 8 oxygen atom around ceria is maximized. This indicates that at the highest lanthanum loading, ceria (or support) interacted more with lanthana, and the role of lanthanum in promoting catalytic activity at active sites is limited. Overall, among all promoted catalysts, the 5Ni + 2La/CeO_2 catalyst exhibited the lowest catalytic activity among the La-promoted catalysts. The degree of graphitization (I_D/I_G) of spent catalysts always remains more than 1, indicating the presence of more disordered carbon than ordered carbon over spent catalysts (Figure S1). The catalyst activity over the current catalyst is compared with the reported catalysts [14,23–28]

and presented in Table 2. The 5Ni + 1.5La/CeO_2 achieved both higher H_2 yield (~65%) and higher H_2/CO (~2.5) than other compared catalysts. A brief investigation of the kinetic results over the 5Ni + 1.5La/CeO_2 catalyst is incorporated into the Supplementary Information as Kinetic Study S5.

Table 2. The comparison of catalytic activity of the catalyst system with the reported catalyst system towards partial oxidation of the methane reaction.

No.	Catalyst	P.L	M.L	RT (°C)	WM (wt.%)	GHSV ($mLh^{-1}g_{cat}^{-1}$)	TOS (Min)	X_{CH_4} (%)	Y_{H_2} (%)	H_2/CO	Ref.
1	5Ni/MgO			600	5	14,400	240	67	64	2.5	[6]
2	2Ni/Al_2O_3			600	2	312,000	120	56	35	2.9	[23]
3	Ni/Al_2O_3		1wt.% ZrO_2	600	2	312,000	120	49	28	2.7	[23]
4	$NiAl_2O_4$	5 wt.% Fe		600	5	14,400	270	69	35	-	[24]
5	2Ni/ZrO_2			600	2	312,000	120	24	2	3.2	[23]
6	5Ni/ZrO_2		30 wt.%TiO_2	600	5	14,400	240	40	30	4.1	[25]
7	5Ni/ZrO_2	2.5 wt.% Sr	30 wt.%TiO_2	600	5	14,400	240	45	47	3.5	[25]
8	5Ni/ZrO_2		30 wt.%TiO_2	600	5	14,400	300	40	30	4.25	[26]
9	5Ni/ZrO_2	2 wt.% Cs	30 wt.%TiO_2	600	5	14,400	300	41	31	3.48	[26]
10	5Ni/ZrO_2	2 wt.% Ce	30 wt.%TiO_2	600	5	14,400	300	43	38	3.84	[26]
11	5Ni/ZrO_2	2 wt.% Sr	30 wt.%TiO^2	600	5	14400	300	46	42	3.72	[26]
12	10Ni/La_2O_3-BFA			850	10	6000	510	88	-	1.25	[14]
13	Bulk-$LaNiO_3$			700	-	21,600	6000	53	-	2.1	[27]
14	15Ni/CeO_2			800	15	(In Pulse)	90	27.6	-	-	[28]
15	5Ni/CeO_2	1.5 wt.% La		600	5	7200	1320	~70	~65	~2.5	*Current Study*

P.L = promoter loading, M.L = support's modifier loading, RT = reaction temperature, WM = active metal wt.%, GHSV = gas hourly space velocity, X_{CH_4} = CH_4 conversion, Y_{H_2} = H_2 yield.

3. Materials and Methods

3.1. Catalyst Preparation

The catalysts were synthesized using the wetness-impregnation method. The details of the preparation method are provided in Supplementary Information S1.

3.2. Catalyst Characterization

The prepared catalysts are well characterized using various characterization techniques such as N_2 physisorption studies, X-ray diffraction, H_2-temperature programmed reduction (TPR), O_2-temperature programmed oxidation (TPO), FT-IR spectroscopy, and Raman spectroscopy. The instrumental specification and analysis procedure details are provided in Supplementary Information S2.

3.3. Catalyst Activity Test

The POM reaction was carried out in a tubular stainless-steel fixed-bed reactor. The details of the catalytic activity tests are provided in Supplementary Information S3.

4. Conclusions

The current study investigates the catalytic performance of an Ni-catalyst supported over ceria (5Ni/CeO_2), and the effect of La-promoter over this catalyst for partial oxidation of methane at 600 °C reaction temperature. The redox property of catalysts is found to be quite effective over a current catalyst system, where active sites are re-generated with

enhanced metal–support interaction under oxidative reaction condition of POM. The entire catalyst system is recognized for production of hydrogen rich syngas ($H_2/CO > 2.5$) during the POM reaction. The La-promoter works by enabling the use of the CO_2 activated in situ from the methane combustion for the oxidation of further CH_4, increasing the methane conversion and H_2 formation compared to the unpromoted catalyst. Loading over 1.5 wt.% gradually reduces the crystallinity of the catalyst structure, and hence exposes an increased amount of active surface sites. 5Ni + 1.5La/CeO_2 presents the highest BET surface area and the highest pore volume (0.19 cm ^{3} /g) among all the catalysts supported on La, which is the main textural merit of this formulation over others. The average pore widths of 5Ni + 1.5La/CeO_2 and 5Ni + 2La/CeO_2 are similar (26.7 nm), but 5Ni + 1.5La/CeO_2 has a better pore volume, and thus more void volume accessible to reactant diffusion and coke storage, resulting in enhanced catalytic activity. It achieves > 65% H_2 yield up to 22 h at 7200 mL h^{-1} $g_{cat}{}^{-1}$ GHSV and 600 °C reaction temperature. At the highest La-loading (2 wt.%), the interaction between La and CeO_2 is enhanced, and the role of La in promoting active sites is limited, which caused inferior catalytic activity compared to the rest of La-loading.

Supplementary Materials: The following supporting information can be downloaded at https://www.mdpi.com/article/10.3390/catal16110962/s1, S1: Catalyst synthesis; S2: Catalyst characterization; S3: Catalyst activity test; S4: Thermogravimetric analysis of spent catalysts; S5: Kinetic study; Figure S1: A schematic diagram of the catalytic reaction setup used for the partial oxidation of methane; Figure S2: XRD patterns of the reduced 5Ni/CeO_2 and 5Ni + xLa/CeO_2 (x = 0.5, 1, 1.5, and 2 wt.%) catalysts in the full 2θ ranges; Figure S3: Raman raw spectra of the spent catalysts; Figure S4: Raman spectra for long TOS of spent 5Ni + 1.5La/CeO_2 catalyst; Figure S5: Methane conversion with error bars and equilibrium line for the catalysts; Figure S6: TGA spent unpromoted and La-promoted Ni/CeO_2 catalysts; Figure S7: Effect of different temperature on methane conversion at fixed GHSV= 14,400 $mLg^{-1}h^{-1}$; Figure S8: Parity plot comparing experimentally calculated CH_4 reaction rates with model-predicted rates from the power-law Arrhenius expression over 5Ni + 1.5La/CeO_2 at GHSV = 14,400 mL g^{-1} h^{-1}. Table S1. Calculated crystallite sizes of CeO_2 support and Ni nanoparticles from XRD data using the Scherrer equation. Table S2. Quantified H_2 consumption from the first H_2-TPR of the unpromoted and La-promoted Ni/CeO_2 catalysts and the bare CeO_2 support. Table S3: Hydrogen balance closure of the catalysts after 300 min on stream.

Author Contributions: Conceptualization, Investigation, Funding acquisition, Writing, W.A.A.-o. and T.S.A.; Resources, Software, Formal analysis, Data curation, M.O.B., A.A.M.A. and R.M.A.; Software, Resources, M.F.A., A.M.M.S. and K.M.A.; writing—review and editing, R.K.; Data curation, Methodology, Writing, reviewing & editing, Conceptualization, Project Administration, A.S.A.-F. All authors have read and agreed to the published version of the manuscript.

Funding: Ongoing Research Funding program, (ORF-2026-469), King Saud University, Riyadh, Saudi Arabia.

Data Availability Statement: All data supporting the findings of this study are presented within the article.

Acknowledgments: The authors acknowledge and appreciate the Ongoing Research Funding Program (ORF-2026-469), King Saud University, Riyadh, Saudi Arabia.

Conflicts of Interest: The authors declare no conflicts of interest.

References

1. Mar, K.A.; Unger, C.; Walderdorff, L.; Butler, T. Beyond CO_2 equivalence: The impacts of methane on climate, ecosystems, and health. *Environ. Sci. Policy* **2022**, *134*, 127–136. [CrossRef]
2. Bentalib, A.S.; BaQais, A.; Ali, F.A.A.; Chaudhary, K.J.; Abahussain, A.A.M.; Jumah, A.B.; Bayazed, M.O.; Saeed, A.M.M.; Kumar, R.; Al-Fatesh, A.S. Hydrogen Production via Dry Reforming of Methane Using a Strontium Promoter over MgO-Supported Ni Catalyst: A Cost-Effective Catalyst System. *Catalysts* **2025**, *15*, 853. [CrossRef]

3. Shan, Y.; Tian, K.; Li, R.; Guan, Y.; Ou, J.; Guan, D.; Hubacek, K. Global methane footprints growth and drivers 1990–2023. *Nat. Commun.* **2025**, *16*, 8184. [CrossRef]
4. International Energy Agency (IEA). Global Methane Tracker 2025—Methane and the 1.5 °C Pathway. 2025. Available online: https://www.iea.org/reports/global-methane-tracker-2025 (accessed on 7 May 2025).
5. Bharadwaj, S.S.; Schmidt, L.D. Catalytic partial oxidation of natural gas to syngas. *Fuel Process. Technol.* **1995**, *42*, 109–127. [CrossRef]
6. Ali, F.A.A.; Chaudhary, K.J.; Ibrahim, A.A.; Alotaibi, N.N.; Alterary, S.S.; Fadhillah, F.; Kumar, R.; Al-Fatesh, A.S. Strontium-Promoted Ni-Catalyst Supported over MgO for Partial Oxidation of Methane: Unveiling a Cost-Effective Catalyst System for Fast Mitigation of Methane. *Catalysts* **2025**, *15*, 814. [CrossRef]
7. Ding, Z.; Chen, S.; Yang, T.; Sheng, Z.; Zhang, X.; Pei, C.; Fu, D.; Zhao, Z.-J.; Gong, J. Atomically dispersed MoNi alloy catalyst for partial oxidation of methane. *Nat. Commun.* **2024**, *15*, 4636. [CrossRef]
8. Chaudhary, M.L.; Kumar, R. Doped Ceria Catalyst System: Catalyzing Carbon Monoxide Transformation (A-Review). *Orient. J. Chem.* **2021**, *37*, 1262–1279. [CrossRef]
9. Khatri, J.; Al-Fatesh, A.S.; Fakeeha, A.H.; Ibrahim, A.A.; Abasaeed, A.E.; Kasim, S.O.; Osman, A.I.; Patel, R.; Kumar, R. Ce promoted lanthana-zirconia supported Ni catalyst system: A ternary redox system for hydrogen production. *Mol. Catal.* **2021**, *504*, 111498. [CrossRef]
10. Jumah, A.B.; Kaydouh, M.-N.; Al-Fatesh, A.S.; Bayazed, M.O.; Fakeeha, A.H.; Ibrahim, A.A.; Abasaeed, A.E.; Chaudhary, K.J.; El Hassan, N. Cerium-induced modification of acid-base sites in Ni-zeolite catalysts for improved dry reforming of methane. *J. Energy Inst.* **2025**, *118*, 101901. [CrossRef]
11. Pal, P.; Singha, R.K.; Saha, A.; Bal, R.; Panda, A.B. Defect-Induced Efficient Partial Oxidation of Methane over Nonstoichiometric Ni/CeO_2 Nanocrystals. *J. Phys. Chem. C* **2015**, *119*, 13610–13618. [CrossRef]
12. Ding, X.; Yang, Y.; Li, Z.; Huang, P.; Liu, X.; Guo, Y.; Wang, Y. Engineering a Nickel–Oxygen Vacancy Interface for Enhanced Dry Reforming of Methane: A Promoted Effect of CeO_2 Introduction into Ni/MgO. *ACS Catal.* **2023**, *13*, 15535–15545. [CrossRef]
13. Xu, Y.; Chen, R.; Lin, H.; Lv, Q.; Liu, B.; Wu, L.; Tan, L.; Dai, Y.; Zong, X.; Tang, Y. Constructing the Ni-O-Ce interface to enhance the activity and stability for partial oxidation of methane to syngas under high temperatures. *J. Catal.* **2024**, *435*, 115545. [CrossRef]
14. Hasanat, A.U.; Khoja, A.H.; Naeem, N.; Al-Anazi, A.; Liaquat, R.; Khan, B.A.; Din, I.U. Thermocatalytic partial oxidation of methane to syngas (H2, CO) production using Ni/La_2O_3 modified biomass fly ash supported catalyst. *Results Eng.* **2023**, *19*, 101333. [CrossRef]
15. Li, B.; Yuan, X.; Li, L.; Li, B.; Wang, X. Reforming Methane with CO_2 over Hierarchical Porous Silica-Supported Nickel Catalysts Modified with Lanthanum Oxide. *Int. J. Energy Res.* **2023**, *2023*, 4201987. [CrossRef]
16. Hao, C.; Qu, Z.; Smith, L.R.; Dummer, N.F.; Qi, H.; Slater, T.J.A.; Zhu, Z.; Zhang, R.; Sun, Z.; Hutchings, G.J. Ce-induced synergistic effect in exsolved perovskite catalyst for highly efficient and robust methane dry reforming. *Nat. Commun.* **2025**, *16*, 10630. [CrossRef]
17. Weber, W.H.; Hass, K.C.; McBride, J.R. Raman study of CeO_2: Second-order scattering, lattice dynamics, and particle-size effects. *Phys. Rev. B* **1993**, *48*, 178–185. [CrossRef]
18. Rui, N.; Zhang, X.; Zhang, F.; Liu, Z.; Cao, X.; Xie, Z.; Zou, R.; Senanayake, S.D.; Yang, Y.; Rodriguez, J.A.; et al. Highly active Ni/CeO_2 catalyst for CO_2 methanation: Preparation and characterization. *Appl. Catal. B Environ.* **2021**, *282*, 119581. [CrossRef]
19. Liu, B.; Li, C.; Zhang, G.; Yao, X.; Chuang, S.S.C.; Li, Z. Oxygen Vacancy Promoting Dimethyl Carbonate Synthesis from CO_2 and Methanol over Zr-Doped CeO_2 Nanorods. *ACS Catal.* **2018**, *8*, 10446–10456. [CrossRef]
20. Schilling, C.; Hofmann, A.; Hess, C.; Ganduglia-Pirovano, M.V. Raman Spectra of Polycrystalline CeO_2: A Density Functional Theory Study. *J. Phys. Chem. C* **2017**, *121*, 20834–20849. [CrossRef]
21. Al-Mubaddel, F.S.; Kumar, R.; Sofiu, M.L.; Frusteri, F.; Ibrahim, A.A.; Srivastava, V.K.; Kasim, S.O.; Fakeeha, A.H.; Abasaeed, A.E.; Osman, A.I. Optimizing acido-basic profile of support in Ni supported La_2O_3+ Al_2O_3 catalyst for dry reforming of methane. *Int. J. Hydrogen Energy* **2021**, *46*, 14225–14235. [CrossRef]
22. Liu, X.; Shao, Y.; Ren, X.; Dong, A.; Li, K.; Zhou, B.; Yang, C.; Liu, Y.; Li, Z. Steam Treatment Promotion on the Performance of Pt/CeO_2 Three-Way Catalysts for Emission Control of Natural Gas-Fueled Vehicles. *Catalysts* **2023**, *14*, 17. [CrossRef]
23. Pompeo, F.; Nichio, N.; Ferretti, O.; Resasco, D. Study of Ni catalysts on different supports to obtain synthesis gas. *Int. J. Hydrogen Energy* **2005**, *30*, 399–1405. [CrossRef]
24. Abasaeed, A.E.; Adil, S.F.; Kuniyil, M.; Ahmed, H.; Ibrahim, A.A.; Fakeeha, A.H.; Al-Fatesh, A.S. Fe_xO_y Nanoparticles Doped Spinel Nickel Aluminate as Partial Oxidation Catalyst: Synthesis, Characterization and Catalytic Evaluation. *Catal. Lett.* **2024**, *154*, 2829–2840. [CrossRef]
25. Alwadai, N.; Abahussain, A.A.M.; Vadodariya, D.M.; Banabdwin, K.M.; Fakeeha, A.H.; Abu-Dahrieh, J.K.; Almuqati, N.S.; Alghamdi, A.M.; Kumar, R.; Al-Fatesh, A.S. Ni–Sr/TiZr for H_2 from methane via POM: Sr loading & optimization. *RSC Adv.* **2024**, *14*, 25273–25288. [CrossRef]

26. Al-Fatesh, A.S.; Vadodariya, D.M.; Banabdwin, K.M.; Ibrahim, A.A.; Fakeeha, A.H.; Adil, S.F.; Kumar, R.; Abahussain, A.A.M. Promoted Ni Catalyst Over Titania-Zirconia Support for Partial Oxidation of Methane: Simple and Practical Catalysts. *Catal. Lett.* **2024**, *154*, 4625–4635. [CrossRef]
27. Duan, Q.; Wang, J.; Ding, C.; Ding, H.; Guo, S.; Jia, Y.; Liu, P.; Zhang, K. Partial oxidation of methane over Ni based catalyst derived from order mesoporous $LaNiO_3$ perovskite prepared by modified nanocasting method. *Fuel* **2017**, *193*, 112–118. [CrossRef]
28. Dong, W.-S.; Jun, K.-W.; Roh, H.-S.; Liu, Z.-W.; Park, S.-E. Comparative Study on Partial Oxidation of Methane over Ni/ZrO_2, Ni/CeO_2 and $Ni/Ce–ZrO_2$ Catalysts. *Catal. Lett.* **2002**, *78*, 215–222. [CrossRef]

Disclaimer/Publisher's Note: The statements, opinions and data contained in all publications are solely those of the individual author(s) and contributor(s) and not of MDPI and/or the editor(s). MDPI and/or the editor(s) disclaim responsibility for any injury to people or property resulting from any ideas, methods, instructions or products referred to in the content.